coatings

MDPI

Brief Report

Tailoring the Ductility of Ti-6Al-4V Titanium Alloy Fabricated by Laser Power Bed Fusion at Liquid Nitrogen Temperature

Bichen Xie [1], Wei Zeng [2], Tian Xia [2,*], Lianbo Wang [1,*] and Kun Chen [1]

[1] School of Materials Science and Engineering, Shanghai Institute of Technology College, Shanghai 201418, China; xiebichen@jiuhe.ltd (B.X.); chk119@sit.edu.cn (K.C.)
[2] JIUHE Frontier Innovations of Science and Technology (Shanghai) Co., Ltd., Shanghai 200240, China; zengwei@jiuhe.ltd
* Correspondence: xiatian@jiuhe.ltd (T.X.); lbwang@sit.edu.cn (L.W.)

Abstract: By tailoring different microstructural features, this study verifies that the laser powder bed fusion (LPBF)-fabricated Ti-6Al-4V titanium alloy with a fully α/β lamellar structure exhibits excellent ductility at liquid nitrogen temperature. HT-800 was obtained by holding at 800 °C for two hours and then furnace-cooled, resulting in a microstructure consisting of residual martensitic α′ phase, lamellar α phase, and particulate β phase. The HT-900 was obtained by holding at 900 °C for two hours and then furnace-cooled, completely eliminating the multi-level martensitic α′ phase generated during the LPBF process and resulting in an α/β lamellar structure. HT-900 achieved an elongation of 11% at liquid nitrogen temperature, a 47% improvement over the HT-800. After low-temperature strain fracture, the proportions of 61.38°<11–20> twin boundaries in the HT-800 and HT-900 were 21.4% and 26.4%, respectively, indicating that a substantial amount of deformation twinning is activated at liquid nitrogen temperature. Twinning induces the activation of slip systems by altering the orientation of surrounding grains. The coordinated plastic deformation of twinning and slip enhances the ductility of the HT-900 at 77 K. The results show that the LPBF-TC4 titanium alloy with a fully α/β lamellar structure exhibits superior, coordinated plastic deformation capabilities at 77 K, maintaining high strength while achieving greater ductility and fracture toughness.

Keywords: laser powder bed fusion; Ti-6Al-4V titanium alloy; liquid nitrogen temperature (77 K); strength-ductility synergy

check for updates

Citation: Xie, B.; Zeng, W.; Xia, T.; Wang, L.; Chen, K. Tailoring the Ductility of Ti-6Al-4V Titanium Alloy Fabricated by Laser Power Bed Fusion at Liquid Nitrogen Temperature. *Coatings* **2024**, *14*, 1528. https://doi.org/10.3390/coatings14121528

Academic Editor: Rafael Comesaña

Received: 7 November 2024
Revised: 21 November 2024
Accepted: 22 November 2024
Published: 3 December 2024

Copyright: © 2024 by the authors. Licensee MDPI, Basel, Switzerland. This article is an open access article distributed under the terms and conditions of the Creative Commons Attribution (CC BY) license (https://creativecommons.org/licenses/by/4.0/).

1. Introduction

Renowned for its high strength-to-weight ratio and excellent corrosion resistance, Ti-6Al-4V (TC4) was most widely used in the aerospace and space industries, where application temperature ranges from extremely low (77 K) to elevated temperature (873 K) [1,2]. However, due to the β-phase content and equiaxed microstructure in as-cast TC4, its ductility at cryogenic temperatures is currently inadequate to fully meet the stringent requirements of space applications [3–6].

Currently, cryogenic titanium alloys in service are predominantly near-α titanium alloys, such as Ti-5Al-2.5Sn [7]. These α-phase alloys are preferred for cryogenic applications due to the lower oxygen sensitivity of α-Ti compared to β-Ti, which reduces embrittlement risks at low temperatures [8]. As temperature decreases into the cryogenic range, the critical resolved shear stress (CRSS) of titanium alloys increases significantly due to an increase in lattice friction, resulting in a marked rise in yield strength [9]. Decreased from 298 K to 77 K, slip activation in α-Ti, and especially in β-Ti phases, becomes increasingly challenging compared to twinning. This is primarily due to the substantial increase in CRSS for slip and twinning, with the rate of increase for slip being notably higher than that for twinning [10].

Notably, the metastable β-Ti alloy Ti-15Mo-2Al exhibits low elongation to failure (EI) at cryogenic temperatures, with values recorded at approximately 4.5% [11]. In contrast, the

lamellar-structured ELI (Extra-Low Interstitial) Ti-5Al-2.5Sn alloy demonstrates superior elongation to failure at 77 K, highlighting its potential for high-performance applications in extreme cryogenic environments [12].

It is well known that TC4 is a dual-phase (α+β) titanium alloy. Tailoring the typical α+β microstructure into near α is a potential advantage. However, TC4 titanium alloys with less than 5% β phase can be fabricated through LPBF [13,14]. Additionally, laser powder bed fusion enables the precise shaping of complex components. The TC4 alloy fabricated by LPBF features a hierarchical acicular martensitic α′ phase structure, resulting from the extremely high cooling rate of the molten pool and the complex thermal cycles. Such a unique microstructural configuration of LPBF-TC4, characterized by acicular martensitic α′ phase and a minimal amount of β phase, provides a foundation for adjusting the microstructural properties. This hierarchical acicular martensitic α′ phase structure in TA15 exhibits an elongation of only 5.2% ± 0.1% at liquid nitrogen temperature [15]. Zang et al. [16] pointed out that a fully lamellar microstructure can endow near-α titanium alloys with excellent plasticity at low temperatures. Sheng et al. [17] found that higher heat treatment temperatures facilitate the decomposition of the martensitic α′ phase and promote the growth of the lamellar structure. The characteristic microstructure generated through LPBF substantially influences the low-temperature performance of TC4 titanium alloy.

In this study, TC4 alloys with a hierarchical martensitic α′ phase and less than 5% β phase content were produced using the LPBF technique. Heat treatment processes were developed below the β-phase transformation point temperature to create two distinct microstructures: one consisting predominantly of residual martensitic α′ phase with a minor fraction of α/β lamellar structure and the other exhibiting a fully developed α/β lamellar structure. The plastic deformation behavior of these two microstructures at low temperatures was systematically analyzed, providing valuable insights for future research on the low-temperature plastic deformation mechanisms of LPBF-processed TC4 alloy.

2. Materials and Method

The LPBF manufacturing system, specifically the HBD 400 model produced by Hanbang Co., Ltd. in Shenzhen, China, is equipped with two 500 W IPG fiber lasers. The processing parameters for the LPBF were set as follows: a laser power of 360 W, a scanning speed of 1200 mm/s, a line spacing of 0.12 mm, a layer rotation of 67°, and a layer thickness of 30 μm. The entire manufacturing process was conducted in an argon environment with an oxygen content below 120 ppm. For the heat treatment process, the LPBF-TC4 was held at 800 °C for 2 h and then cooled in the furnace, designated as HT-800. Similarly, the LPBF-TC4 was held at 900 °C for 2 h and subsequently cooled in the furnace, designated as HT-900.

The samples produced by LPBF were ground and polished, followed by etching with Keller's reagent (comprising 1.0% HF, 1.5% HCl, 2.5% HNO3, and 95.0% distilled water) for observation under an optical microscope (OM) (OPTIKA IM 3 MET, Bergamo, Italy). Additionally, a field emission scanning electron microscope (FESEM) (NOVA NanoSEM-230, Sydney, NSW, Australia), along with an electron backscatter diffraction (EBSD) system (OXFORD Symmetry-S3, London, UK), was utilized to inspect the microstructure of the samples. Tensile tests were conducted on HT-800 and HT-900 at a liquid nitrogen temperature of 77 K using an MTS CMT5150 low-temperature tensile testing machine with a constant strain rate of 5×10^{-4} s^{-1}.

3. Results and Discussion

The XRD patterns of the HT-800, HT-900, and LPBF-TC4 are shown in Figure 1a, with all specimens exhibiting diffraction peaks corresponding to the HCP phase. The HCP phase consists of α and α′ martensite, and despite their similar lattice parameters, slight differences are observable in the XRD spectra [18]. This is attributed to rapid cooling inhibiting solute diffusion and enriching the α′ martensite in V and Mo, leading to crystal structure distortion and broadening of the diffraction peaks [19]. By combining Figure 1b,c,

it can be observed that the HCP diffraction peaks in LPBF-TC4 are entirely α′ martensite, which forms due to the extremely high cooling rate and complex thermal cycles during the LPBF process. This results in a hierarchical metastable phase (acicular martensite α′) with less than 5% β phase so that no diffraction peaks for the β phase are observed in the XRD spectrum. The HCP diffraction peaks in the HT-800 consist of residual α′ and a small amount of α phase. For the HT-900, the HCP peaks are entirely α phase. Comparing the heat treatment schemes of HT-800 and HT-900, a weak β phase diffraction peak can be observed at the 42° position in both. In HT-800, there is a significant amount of residual α′ phase, lamellar α phase, and a small amount of dispersed β phase, whereas in HT-900, the α′ phase has completely transformed into a fully α/β lamellar structure. This is because the decomposition rate of the martensite α′ phase accelerates with increasing temperature; at the same holding time, higher temperatures yield larger dimensions of the lamellar structure [17].

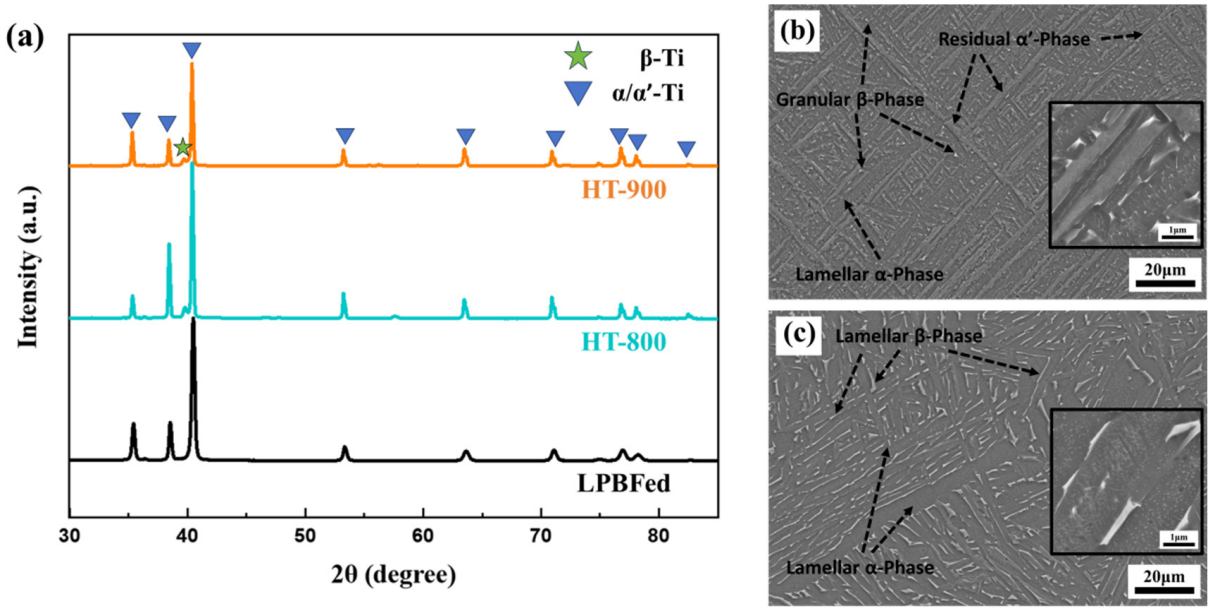


Figure 1. (**a**) XRD patterns of the HT-800, HT-900, and LPBFed.; SEM micrograph of the microstructure of the (**b**) HT-800, (**c**) HT-900.

Tensile tests were conducted at liquid nitrogen temperature (77 K) on samples subjected to HT-800 and HT-900 heat treatment processes, with results presented in Figure 2a. Under the HT-800 heat treatment conditions, the samples exhibited a tensile strength of 1599 MPa, a yield strength of 1565 MPa, and an elongation of 7.5%. For the HT-900 treated samples, the tensile strength was 1489 MPa, the yield strength was 1473 MPa, and the elongation reached 11%, representing a 47% increase compared to the HT-800. Figure 2b,c show the microscopic morphology at the fracture surfaces. In the HT-800, large cleavage steps, tear ridges, and smaller dimples are evident, with cracks propagating along the large acicular martensitic α′ phases until the final fracture. In contrast, the HT-900 shows almost no cleavage steps but presents a greater number of larger dimples. Fracture morphology analysis reveals that the HT-800 exhibits a mixed fracture mode, while the HT-900 demonstrates a ductile fracture mode. The average dimple size for the HT-800 is 1.02 μm, while that for the HT-900 is 6.93 μm. The comparison of microscopic morphology at the fracture surface and dimple size clearly indicates that the low-temperature toughness of the HT-900 is superior to that of the HT-800, which is consistent with the tensile test results. This also confirms that the TC4 alloy with a fully α/β lamellar structure possesses better plastic deformation capability at liquid nitrogen temperatures.

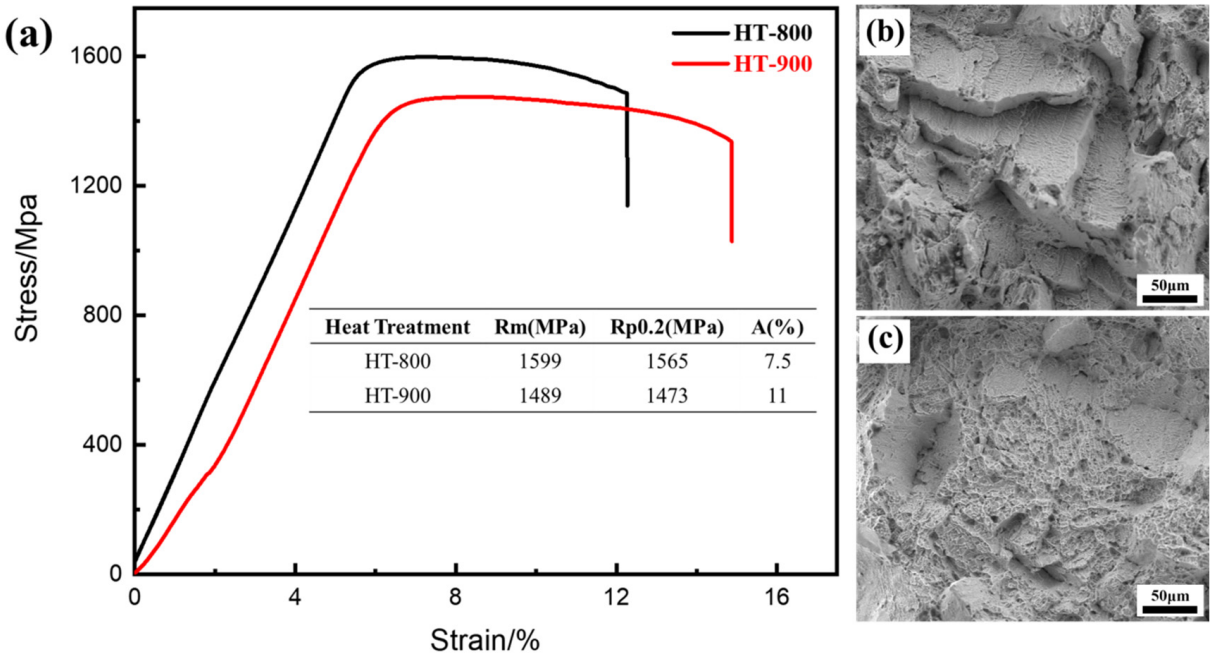


Figure 2. (**a**) Liquid nitrogen temperature tensile test results and data summary of HT-800 and HT-900.; fracture SEM morphology of the (**b**) HT-800 and (**c**) HT-900.

Figure 3a,b show the IMMA images of the HT-800 and HT-900 before deformation. It can be observed that, prior to deformation, the HT-900 contains a higher number of recrystallized grains. This suggests that the elevated heat treatment temperature not only completely eliminates the martensitic α′ phase but also promotes dislocation recovery, grain recrystallization, and partial grain sub-structuring [20]. These changes help retain the material's strength while enhancing its plastic deformation capacity. Observing the IMMA images of the deformed in Figure 3c,d and the IMMA proportion distribution in Figure 3e, the proportions of deformed grains in the HT-800 and HT-900 after deformation are 53% and 82.3%, respectively. The higher proportion of deformed grains in the HT-900 is attributed to the more active dislocation motion in the recrystallized grains, where dislocations can pass through the interfaces of the α/β lamellar structure [21], leading to a more uniform stress distribution in the sample and enhancing its ability for coordinated deformation.

Figure 3f–i present the orientation difference distribution maps of the HT-800 and HT-900 before and after deformation. It can be observed that the orientation difference distribution of both samples is quite similar prior to deformation, with the HT-900 exhibiting slightly lower proportions of low-angle grain boundaries (LAGBs). After deformation, the proportions of LAGBs in the HT-800 and HT-900 are 15.2% and 24.2%, respectively. Both samples show an increase in the proportion of LAGBs after deformation, but the increase is more pronounced in the HT-900. This is primarily attributed to the activation of more dislocations and twins within the α/β lamellar structure during deformation [15], resulting in a more uniform stress distribution in the HT-900 and a greater number of grains participating in deformation, which is consistent with the IMMA results.

At room temperature, slip is the primary deformation mechanism during the plastic deformation phase in titanium alloys. However, at low temperatures, twinning tends to occur prior to slip due to differences in the critical resolved shear stress (CRSS) variation with temperature for slip and twinning [15,21]. To determine the activated slip systems, we compared the Schmid factor (SF) distribution across different slip systems in the HT-800 and HT-900 after strain fracture, as shown in Figure 4a–h, and calculated the average SF values for each slip system, as depicted in Figure 4i. The Schmid factors for all slip systems in the HT-900 are higher than those in the HT-800, indicating that at low temperatures, the grains within the HT-900 are more likely to activate slip systems to facilitate coordinated

deformation. The significant difference in SF between basal slip and <a> prismatic slip suggests that these two slip systems are more easily activated in the α/β lamellar structure of TC4 at liquid nitrogen temperature.

At 77 K, twinning is expected to initiate preferentially due to its relatively low CRSS [2], subsequently rotating nearby grains toward orientations more favorable for slip activation, thereby enabling coordinated plastic deformation through twinning-slip synergy. As shown in Figure 4j,k, the proportions of 61.38°<11–20> twin boundaries in the HT-800 and HT-900 after strain fracture are 21.4% and 26.4%, respectively. The acicular martensitic α′ phase has narrower dislocation channels, which are unfavorable for the initiation of twinning and slip, while the larger α lamellae are more conducive to both twinning and slip, with twins capable of traversing α/β interfaces [16,21]. Consequently, the HT-900 with a fully α/β lamellar structure exhibits a higher proportion of twinning, leading to enhanced twinning-slip coordinated plastic deformation. This manifests macroscopically as greater elongation at liquid nitrogen temperature (77 K).

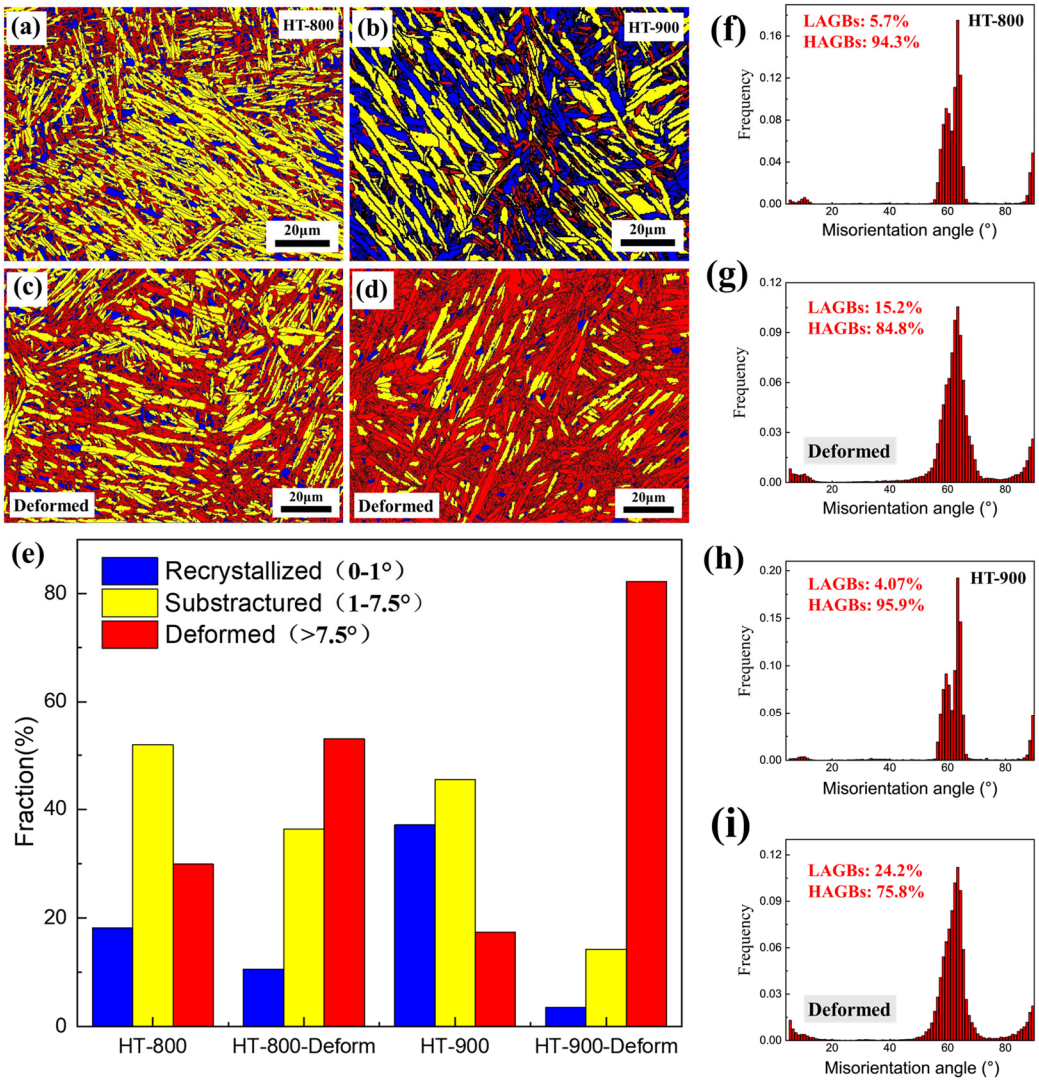


Figure 3. (**a**–**d**) IAMA map and (**e**) IAMA proportional fraction diagram of HT-800 and HT-900, Orientation difference distribution maps before and after deformation of (**f**,**g**) HT-800, (**h**,**i**) HT-900.

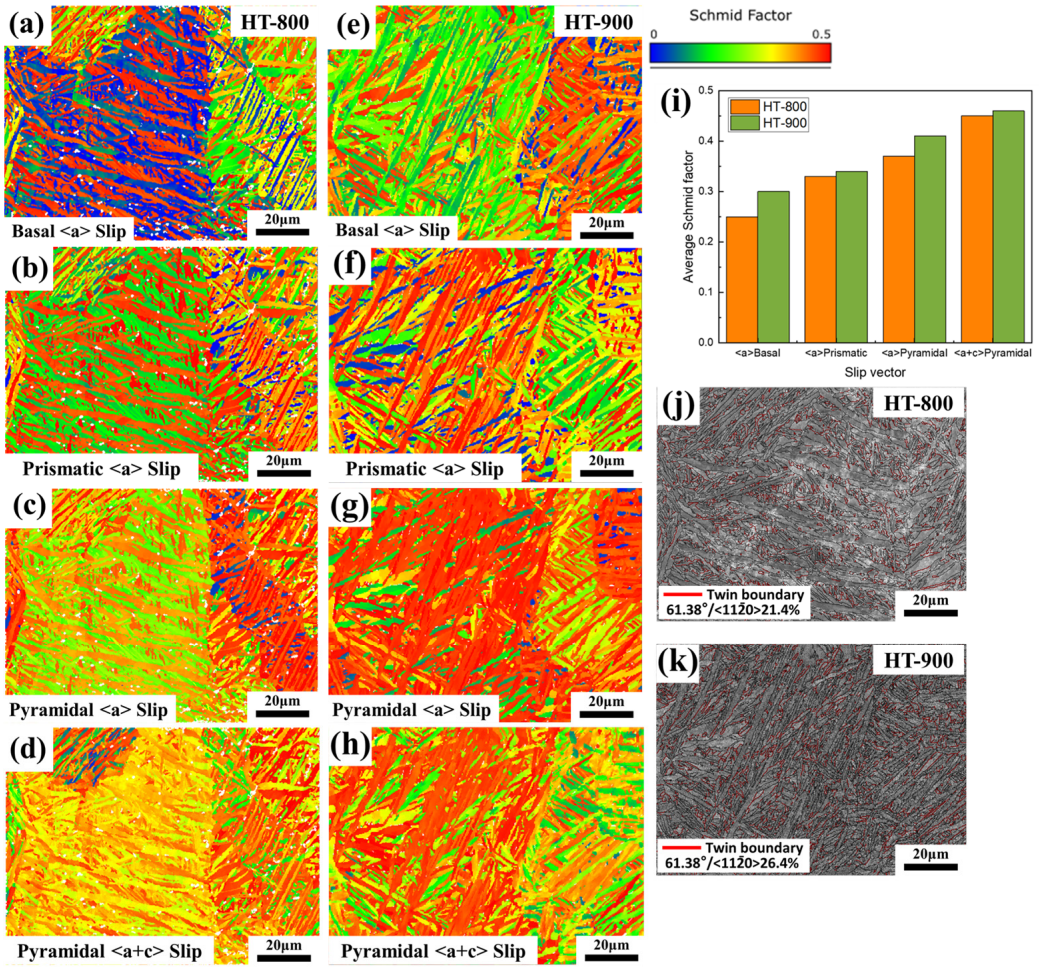


Figure 4. Schmid factor distribution from basal <a>, prismatic <a>, pyramidal <a>, and pyramidal <c+a> slips at (**a**–**d**) HT-800 and (**e**–**h**) HT-900 after straining to fracture; (**i**) average SF values of individual slip systems of the deformed after straining to fracture at HT-800 and HT-900; and twin boundary map after strain fracture at (**j**) HT-800 and (**k**) HT-900.

4. Conclusions

This study fabricated a TC4 titanium alloy using the laser powder bed fusion (LPBF) technique. Two heat treatment regimes, HT-800 and HT-900, were designed below the β-phase transition point. The microstructure of the HT-800 consists of residual martensitic α′ phase, lamellar α phase, and dispersed β-phase particles, while the HT-900 features a fully α/β lamellar structure.

1. The tensile results at liquid nitrogen temperature indicate that the HT-800 exhibits a tensile strength of 1599 MPa, a yield strength of 1565 MPa, and an elongation of 7.5%. In contrast, the HT-900 shows a tensile strength of 1489 MPa, a yield strength of 1473 MPa, and an elongation of 11%.
2. The elongation of the HT-900 at liquid nitrogen temperature surpasses that of the HT-800 by 47%. This remarkable elongation is accompanied by high strength, demonstrating that the fully α/β lamellar structure of TC4 is particularly advantageous for applications in low-temperature environments.
3. After low-temperature strain fracture, the proportions of low-angle grain boundaries (LAGBs) in the HT-800 and HT-900 are 15.2% and 24.2%, respectively, with deformed grain counts of 53% and 82.3%. The proportions of 61.38°<11–20> twin boundaries in the HT-800 and HT-900 are 21.4% and 26.4%, respectively.
4. At liquid nitrogen temperature, the critical resolved shear stress (CRSS) for twinning is lower than that for slip, resulting in significant deformation twinning in the HT-900,

which activates the slip systems. The Schmid factors for all slip systems in the HT-900 exceed those in the HT-800 due to the latter's martensitic α′ phase having fewer dislocation pathways. In contrast, the α lamellar structure facilitates both dislocation slip and twinning. The coordinated deformation of twinning and slip allows the HT-900 to better resist plastic deformation at liquid nitrogen temperature, leading to superior low-temperature elongation.

Author Contributions: Conceptualization, B.X. and W.Z.; methodology, W.Z.; software, B.X.; formal analysis, K.C.; investigation, B.X.; resources, T.X. and L.W.; data curation, B.X.; writing—original draft preparation, B.X.; writing—review and editing, W.Z.; visualization, L.W.; project administration, T.X.; funding acquisition, T.X. and K.C. All authors have read and agreed to the published version of the manuscript.

Funding: This research received no external funding.

Institutional Review Board Statement: Not applicable.

Informed Consent Statement: Not applicable.

Data Availability Statement: Data is contained within the article.

Conflicts of Interest: Author Tian Xia, Wei Zeng were employed by JIUHE Frontier Innovations of Science and Technology (Shanghai) Co., Ltd., located in Shanghai, 200240, China. The remaining authors declare that the research was conducted in the absence of any commercial or financial relationships that could be construed as a potential conflict of interest.

References

1. Banerjee, D.; Williams, J.C. Perspectives on Titanium Science and Technology. *Acta Mater.* **2013**, *61*, 844–879. [CrossRef]
2. Reytier, M.; Kircher, F.; Levesy, B. Characterization of titanium alloys for cryogenic applications. In *AIP Conference Proceedings*; American Institute of Physics: New York, NY, USA, 2002; Volume 614, pp. 76–83.
3. Khan, M.A.; Imran Jaffery, S.H.; Khan, M.; Alruqi, M. Machinability analysis of Ti-6Al-4V under cryogenic condition. *J. Mater. Res. Technol.* **2023**, *25*, 2204–2226. [CrossRef]
4. Matsumoto, H.; Yoneda, H.; Sato, K.; Kurosu, S.; Maire, E.; Fabregue, D.; Konno, T.J.; Chiba, A. Room-temperature ductility of Ti–6Al–4V alloy with α′ martensite microstructure. *Mater. Sci. Eng. A* **2011**, *528*, 1512–1520. [CrossRef]
5. Zhao, W.; Su, W.; Li, L.; Fang, D.; Chen, N. Evolution of Mechanical Properties of Ti–6Al–4V Alloy in the Temperature Range of 20 to −196 °C. *Met. Mater. Int.* **2021**, *27*, 3214–3224. [CrossRef]
6. Kozadaeva, M.; Surmeneva, M.; Khrapov, D.; Rybakov, V.; Surmenev, R.; Koptyug, A.; Vladescu Dragomir, A.; Cotrut, C.M.; Tyurin, A.; Grubova, I. Assessment of Microstructural, Mechanical and Electrochemical Properties of Ti-42Nb Alloy Manufactured by Electron Beam Melting. *Materials* **2023**, *16*, 4821. [CrossRef]
7. Zhang, L.; Dong, P.; Chen, S.; Wang, Y.; Yao, H.; Zeng, Y.; Chen, J. Effect of process induction on densification behavior, microstructure evolution and mechanical properties of Ti-5Al-2.5Sn ELI fabricated by laser powder bed melting. *J. Alloys Compd.* **2023**, *945*, 169292. [CrossRef]
8. Zang, M.C.; Niu, H.Z.; Yu, J.S.; Zhang, H.R.; Zhang, T.B.; Zhang, D.L. Cryogenic tensile properties and deformation behavior of a fine-grained near alpha titanium alloy with an equiaxed microstructure. *Mater. Sci. Eng. A* **2022**, *840*, 142952. [CrossRef]
9. Zhao, B.; Huang, P.; Zhang, L.; Li, S.; Zhang, Z.; Yu, Q. Temperature Effect on Stacking Fault Energy and Deformation Mechanisms in Titanium and Titanium-aluminium Alloy. *Sci. Rep.* **2020**, *10*, 3086. [CrossRef] [PubMed]
10. Zang, M.C.; Niu, H.Z.; Zhang, H.R.; Tan, H.; Zhang, D.L. Cryogenic tensile properties and deformation behavior of a superhigh strength metastable beta titanium alloy Ti–15Mo–2Al. *Mater. Sci. Eng. A* **2021**, *817*, 141344. [CrossRef]
11. Ghisi, A. Mechanical characterization of Ti–5Al–2.5Sn ELI alloy at cryogenic and room temperatures. *Int. J. Fract.* **2007**, *146*, 61–77. [CrossRef]
12. Kumar, P.; Prakash, O.; Ramamurty, U. Micro-and meso-structures and their influence on mechanical properties of selectively laser melted Ti-6Al-4V. *Acta Mater.* **2018**, *154*, 246–260. [CrossRef]
13. Yan, X.; Yin, S.; Chen, C.; Huang, C.; Bolot, R.; Lupoi, R.; Kuang, M.; Ma, W.; Coddet, C.; Liao, H.; et al. Effect of heat treatment on the phase transformation and mechanical properties of Ti6Al4V fabricated by selective laser melting. *J. Alloys Compd.* **2018**, *764*, 1056–1071. [CrossRef]
14. Wang, Q.; Liu, X.; Ren, Y.; Song, M.; Baker, I.; Wu, H. Microstructural evolution and cryogenic and ambient temperature deformation behavior of the near-α titanium alloy TA15 fabricated by laser powder bed fusion. *J. Alloys Compd.* **2024**, *1001*, 175075. [CrossRef]
15. Zang, M.C.; Niu, H.Z.; Liu, S.; Yu, J.S.; Zhang, H.R.; Zhang, D.L. Achieving high tensile strength-ductility synergy of a fully-lamellar structured near alpha titanium alloy at extra-low temperatures. *J. Alloys Compd.* **2022**, *923*, 166363. [CrossRef]

16. Cao, S.; Hu, Q.; Huang, A.; Chen, Z.; Sun, M.; Zhang, J.; Fu, C.; Jia, Q.; Lim, C.V.S.; Boyer, R.R.; et al. Static coarsening behaviour of lamellar microstructure in selective laser melted Ti–6Al–4V. *J. Mater. Sci. Technol.* **2019**, *35*, 1578–1586. [CrossRef]
17. Cao, S.; Chu, R.; Zhou, X.; Yang, K.; Jia, Q.; Lim, C.V.S.; Huang, A.; Wu, X. Role of martensite decomposition in tensile properties of selective laser melted Ti-6Al-4V. *J. Alloys Compd.* **2018**, *744*, 357–363. [CrossRef]
18. Yang, J.; Yu, H.; Yin, J.; Gao, M.; Wang, Z.; Zeng, X. Formation and control of martensite in Ti-6Al-4V alloy produced by selective laser melting. *Mater. Des.* **2016**, *108*, 308–318. [CrossRef]
19. Jiang, J.; Ren, Z.; Ma, Z.; Zhang, T.; Zhang, P.; Zhang, D.Z.; Mao, Z. Mechanical properties and microstructural evolution of TA15 Ti alloy processed by selective laser melting before and after annealing. *Mater. Sci. Eng. A* **2020**, *772*, 138742. [CrossRef]
20. Anne, B.R.; Okuyama, Y.; Morikawa, T.; Tanaka, M. Activated slip systems in bimodal Ti–6Al–4V plastically deformed at low and moderately high temperatures. *Mater. Sci. Eng. A* **2020**, *798*, 140211. [CrossRef]
21. Zhong, H.Z.; Zhang, X.Y.; Wang, S.X.; Gu, J.F. Examination of the twinning activity in additively manufactured Ti-6Al-4V. *Mater. Des.* **2018**, *144*, 14–24. [CrossRef]

Disclaimer/Publisher's Note: The statements, opinions and data contained in all publications are solely those of the individual author(s) and contributor(s) and not of MDPI and/or the editor(s). MDPI and/or the editor(s) disclaim responsibility for any injury to people or property resulting from any ideas, methods, instructions or products referred to in the content.